Partial-depth lock-release flows

M. A. Khodkar, M. M. Nasr-Azadani, and E. Meiburg
Department of Mechanical Engineering, University of California, Santa Barbara, Santa Barbara, California 93106, USA
(Received 2 February 2017; published 28 June 2017)

We extend the vorticity-based modeling concept for stratified flows introduced by Borden and Meiburg [Z. Borden and E. Meiburg, J. Fluid Mech. **726**, R1 (2013)] to unsteady flow fields that cannot be rendered quasisteady by a change of reference frames. Towards this end, we formulate a differential control volume balance for the conservation of mass and vorticity in the fully unsteady parts of the flow, which we refer to as the differential vorticity model. We furthermore show that with the additional assumptions of locally uniform parallel flow within each layer, the unsteady vorticity modeling approach reproduces the familiar two-layer shallow-water equations. To evaluate its accuracy, we then apply the vorticity model approach to partial-depth lock-release flows. Consistent with the shallow water analysis of Rottman and Simpson [J. W. Rottman and J. E. Simpson, J. Fluid Mech. **135**, 95 (1983)], the vorticity model demonstrates the formation of a quasisteady gravity current front, a fully unsteady expansion wave, and a propagating bore that is present only if the lock depth exceeds half the channel height. When this bore forms, it travels with a velocity that does not depend on the lock height and the interface behind it is always at half the channel depth. We demonstrate that such a bore is energy conserving. The differential vorticity model gives predictions for the height and velocity of the gravity current and the bore, as well as for the propagation velocities of the edges of the expansion fan, as a function of the lock height. All of these predictions are seen to be in good agreement with the direct numerical simulation data and, where available, with experimental results. An energy analysis shows lock-release flows to be energy conserving only for the case of a full lock, whereas they are always dissipative for partial-depth locks.

DOI: 10.1103/PhysRevFluids.2.064802

I. INTRODUCTION

Gravity currents are predominantly horizontal flows driven by hydrostatic pressure differences due to density gradients in a gravitational field [1–4]. The development of simplified models for predicting the front velocity of such gravity currents has a long history, dating back to the pioneering work of von Kármán three quarters of a century ago [5], as well as subsequent investigations by Benjamin [6] and Shin *et al.* [7]. As a common feature, all of the above models are based on the integral laws for the conservation of mass of the dense and light fluids, as well as the conservation of overall horizontal momentum. An energy-related empirical argument is then employed along a certain streamline in order to quantify the head loss across the gravity current front so that a closed system of algebraic equations is obtained. The key difference among the individual models lies in where this energy argument is invoked.

More recently, an alternative approach for modeling Boussinesq gravity currents was proposed by Borden and Meiburg [8] (see Fig. 1). Starting from the Euler equations for the conservation of horizontal and vertical momentum, the authors eliminate the pressure variable by focusing on the vorticity form of the Euler equation, thereby avoiding the need for a head loss closure assumption. They furthermore assume that the flow is steady in the reference frame moving with the current front and that the gravity current fluid is at rest in this reference frame. In integral form, the authors thus obtain, for the control volume $BCDE$,

$$\oint \omega \mathbf{u} \cdot \mathbf{n}\, dS = \iint -g' \frac{\partial \rho^*}{\partial x} dA, \tag{1}$$

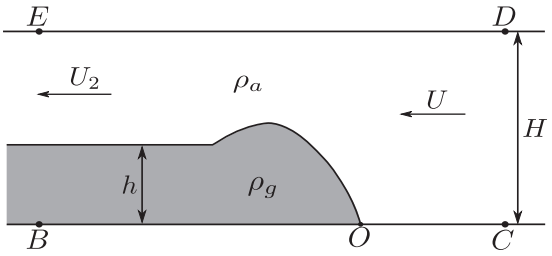

FIG. 1. Schematic of a gravity current of thickness h propagating with velocity U into a channel of depth H, in a reference frame moving with the current front.

where ω and $\mathbf{u}$ represent the vorticity normal to the plane and the velocity vector, respectively; g' is the reduced gravity defined as $g(\rho_g - \rho_a)/\rho_a$; ρ^* denotes the dimensionless density $(\rho - \rho_a)/(\rho_g - \rho_a)$; and dA, dS, and $\mathbf{n}$ indicate a differential area within the control volume, a differential length along the boundaries of the control volume, and the unit outer normal vector to the control volume boundaries. The equation hence states that for a steady solution to exist, the rate at which vorticity is being convected out of the control volume across boundary BE has to equal the rate at which it is being generated within the control volume by baroclinic production. The vorticity outflux can be evaluated as the vortex sheet strength U_2 times its principal velocity $U_2/2$ [9]. Thus the integral form of the inviscid vorticity conservation equation immediately leads to

$$\tfrac{1}{2}U_2^2 = g'h. \tag{2}$$

When combined with the mass conservation equation for the ambient stream

$$UH = U_2(H - h), \tag{3}$$

we thus obtain the gravity current velocity as

$$\frac{U}{\sqrt{g'H}} = \sqrt{2\alpha}(1 - \alpha), \tag{4}$$

where $\alpha = h/H$. This vorticity-based approach yields results that are different from but quantitatively similar to those obtained with the model of Benjamin [6],

$$\frac{U}{\sqrt{g'H}} = \sqrt{\frac{2 - \alpha}{1 + \alpha}(1 - \alpha)\alpha}. \tag{5}$$

In spite of their quantitatively similar predictions, there exist a few subtle differences between the models of Benjamin [6] and Borden and Meiburg [8], on which we briefly comment in the following.

A. Commonalities and differences of Benjamin's and the vorticity model

Both Benjamin [6] and Borden and Meiburg [8] aim to establish relationships between the flow properties far up- and downstream of the gravity current front, by invoking *integral* conservation laws. Towards this end, both models make certain assumptions such as steady, uniform parallel flow far up- and downstream, slip top and bottom walls, a current that is at rest in the moving reference frame, and a sharp interface. These are, of course, simplifications of the true experimental situation, which is typically unsteady, dissipative, and with a diffusive interface. Both models satisfy the integral form of the continuity equation for the ambient fluid and both models satisfy the integral conservation equation for horizontal momentum, without viscous forces along the top and bottom walls. Up to this point, the models are identical.

The difference arises in how a third equation is obtained. Benjamin [6] accomplishes this by employing Bernoulli's equation along the streamline upstream of the stagnation point, meaning that

a *local* form of the inviscid horizontal momentum equation is employed simultaneously with the integral form of the horizontal momentum equation. By evaluating Bernoulli's equation along the upper wall, it is then shown that a head loss exists, unless $h/H = 0.5$. While the model assumes hydrostatic pressure profiles far up- and downstream of the gravity current front, it makes no attempt to incorporate the conservation of vertical momentum across the gravity current front, where the flow is nonhydrostatic as the ambient fluid is accelerated upward near the front and subsequently turned back into the horizontal direction by the upper wall, with implications for the pressure profile along this wall.

The vorticity model takes a different approach in order to obtain a third equation. It incorporates the principle of vertical momentum conservation by writing the integral form of the inviscid vorticity conservation equation between the up- and downstream boundaries, as discussed above. By combining this integral vorticity equation with the integral continuity equation we are able to determine the front velocity of the gravity current without any knowledge of the pressure field. This finding is consistent with the well known fact that in two-dimensional numerical simulations, the gravity current velocity can be determined from the stream-function–vorticity form of the Navier-Stokes equations, without solving for the pressure [10]. The observation that the front velocity is solely a function of the conservation of mass and vorticity demonstrates the importance of incorporating vertical momentum conservation into the derivation. Once the front and ambient velocities have been determined from the integral conservation laws for mass and vorticity alone, the vorticity model evaluates the pressure variable directly from the integral conservation relation for horizontal momentum, without invoking Bernoulli's equation anywhere in the flow. We note that by employing the integral form of the inviscid vorticity equation, the vorticity model neglects the diffusive spreading of the interfacial vortex sheet, as well as any diffusive flux of vorticity across the top and bottom walls. For gravity currents propagating into shear, Nasr-Azadani and Meiburg [11] compared direct numerical simulation (DNS) results for the traditional slip condition along the walls $\frac{\partial u}{\partial y} = 0$ with those for a no-flux condition $\frac{\partial^2 u}{\partial y^2} = 0$ and found the differences to be negligible.

If one were to integrate Bernoulli's equation around the closed curve $BOCDEB$, assuming hydrostatic pressure along the in- and outflow boundaries, one recovers Eq. (2). However, this does *not* imply that the vorticity model effectively employs Bernoulli's equation. Rather, it merely reflects the fact that the front and ambient velocities can be evaluated without any knowledge of the pressure field and that they do not uniquely determine the pressure field, so different pressure fields can be constructed that are compatible with these given front and ambient velocities. For example, if identical head losses exist along the upper and lower walls, one still recovers Eq. (2). Hence, the correct way of evaluating the pressure is not from Bernoulli's law, but from the integral horizontal momentum equation for the entire control volume. It is easily shown by substitution that the pressure values obtained from integrating Bernoulli's law violate the integral conservation equation for horizontal momentum, except for the case of $h/H = 0.5$.

We can hence summarize the key commonalities and differences between the models by Benjamin [6] and Borden and Meiburg [8] as follows: The vorticity model is based on the three integral conservation laws for (i) mass of the ambient fluid, (ii) horizontal momentum, and (iii) vorticity. It does not apply Bernoulli's law anywhere, either explicitly or implicitly. The model of Benjamin [6], on the other hand, is based on (i) the integral form of the continuity equation for the ambient fluid, (ii) the integral conservation law for horizontal momentum, and (iii) Bernoulli's equation along the stagnation point streamline. As mentioned above, despite these subtle differences, the quantitative predictions by the two models are quite close to each other and they can be viewed as somewhat different approximations of the true experimental situation.

B. Problem setup

As described above, the work by Borden and Meiburg [8] had introduced the vorticity modeling approach for a gravity current front in an integral form, for a flow field that can be rendered steady by shifting to a reference frame moving with the front. Khodkar *et al.* [12] subsequently extended this approach to unsteady flow fields composed of several fronts propagating at different velocities.

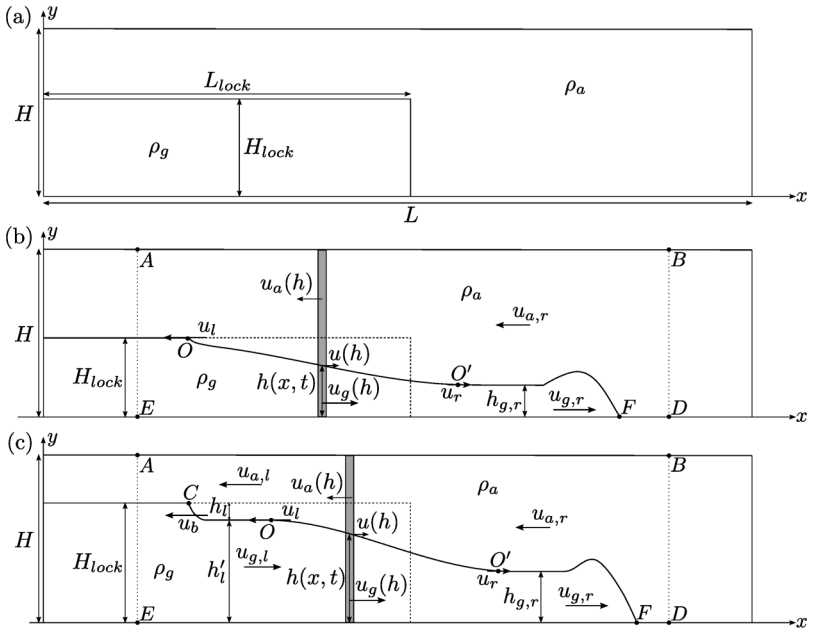

FIG. 2. Schematic of a partial-depth lock-release flow. (a) Initially, the dense fluid is confined to a lock of length L_{lock} and height H_{lock}. (b) Upon removal of the gate, the heavy fluid of density ρ_g forms a gravity current with quasisteady propagation velocity $u_{g,r}$ and height $h_{g,r}$. The light ambient fluid of density ρ_a forms a return flow. For $H_{\text{lock}} < H/2$, the quasisteady gravity current is connected to the lock fluid by an unsteady expansion fan. (c) For $H_{\text{lock}} > H/2$, a quasisteady bore of height h_l and velocity u_b forms at the left edge of the expansion fan. The thin gray rectangles in (b) and (c) indicate the differential control volumes employed to derive the conservation laws.

They accomplished this by analyzing each front separately in a reference frame that renders it steady and by then matching the solutions in the different reference frames.

Within the present investigation, we will extend the vorticity modeling approach to fully unsteady flows, i.e., to flow fields that cannot be constructed by superimposing and then matching a finite number of quasisteady components. In order to develop the modeling framework, we will focus on the canonical lock-release configuration (see Fig. 2). A tank of length L and height H is divided into two compartments: A rectangular lock with length L_{lock} and height H_{lock} initially contains the heavy fluid of density ρ_g, while the remainder of the space is occupied by the light ambient fluid of density ρ_a. Initially, these two immiscible fluids are separated by a gate. Upon removal of the gate, the heavy fluid forms a gravity current with velocity $u_{g,r}$ and height $h_{g,r}$ that travels towards the right along the bottom wall. This gravity current is connected to the lock fluid by a rarefaction or expansion wave of height $h(x,t)$, either directly, as in Fig. 2(b) or via a bore, as in Fig. 2(c). The left and right edges of this expansion wave travel with speeds u_l and u_r, respectively. Note that positive velocity values correspond to the directions of the arrows in Fig. 2. We aim to analyze the flow before the left edge of the rarefaction wave or the bore interacts with the left wall. Within the rarefaction wave, the dense fluid has a velocity $u_g(h)$. Concurrently, the ambient forms a left-propagating return flow with velocity $u_{a,r}$ above the gravity current and $u_a(h)$ above the rarefaction wave. The velocity $u(h)$ with which the interface location of height h moves horizontally varies from $-u_l$ to u_r within the rarefaction wave. If the lock height H_{lock} equals the tank height H, we refer to the flow as a full-depth lock-release current, while for $H_{\text{lock}} \neq H$ we obtain a partial-depth lock-release flow.

Based on the two-layer shallow-water equations, Rottman and Simpson [13] proposed a model for partial-depth lock-release flows that includes the rarefaction wave behind the gravity current. Since the shallow-water equations cannot directly model the gravity current front, its effect is accounted

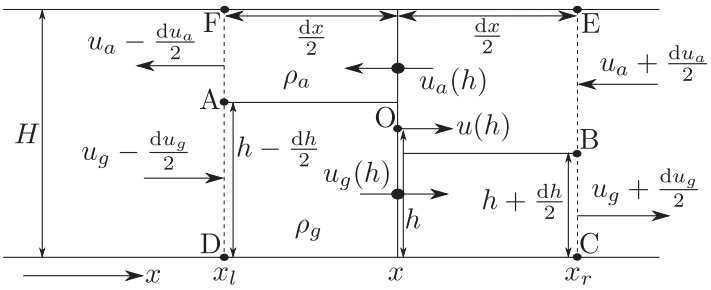

FIG. 3. Magnified form of the differential control volume in Fig. 2. The entire control volume $DCEF$ moves with the velocity $u(h)$ of the steplike variation in interface height at location O, so the flow within the control volume is quasisteady. We assume locally uniform flow within each layer at the in- and outflow boundaries. Note that $dh < 0$.

for by an empirically modified front condition. For $H_{\text{lock}}/H \leqslant 0.5$, predictions by this model agree closely with experimental observations. While the shallow-water model correctly predicts that a left-propagating bore forms for $H_{\text{lock}}/H > 0.5$, this bore is not accounted for in the model, so the agreement between the model and experiments deteriorates in this parameter range.

Shin *et al.* [7] proposed a model that accounts for the entire flow field, i.e., both for the rarefaction wave and for the right- and left-propagating fronts. They employed a control volume approach that conserves mass and horizontal momentum and also enforces the unsteady Bernoulli equation along the top boundary. The authors furthermore assumed the interface height to be uniform along the rarefaction wave and to change abruptly from $h_{g,r}$ to H_{lock} at the left edge. In this way, they obtained for the gravity current speed in the Boussinesq limit

$$\frac{u_{g,r}}{\sqrt{g'H}} = \frac{1}{2}\sqrt{\frac{H_{\text{lock}}(2H - H_{\text{lock}})}{H^2}}. \tag{6}$$

The experiments by Shin *et al.* [7] furthermore confirmed that it is possible for gravity currents with $h_{g,r}/H > 0.347$ to form, whereas Benjamin [6] had suspected that such currents "would be difficult, if not impossible, to produce experimentally." The authors attributed this observation to the momentum and energy transfer between the rarefaction wave and the current front, which is not accounted for in Benjamin's model.

The present study proposes a differential vorticity-based approach for analyzing the entire unsteady flow field, including the gravity current, the rarefaction wave, and the internal bore. Section II constructs the vorticity-based model and obtains predictions for the speed and height of the gravity current, as well as for the velocities of the left and right edges of the expansion fan. Section III presents DNSs and Sec. IV compares them to the model predictions as well as to theoretical and experimental findings of earlier studies. Section V describes an *a posteriori* analysis of the flow energetics, while Sec. VI summarizes the findings and gives some concluding remarks.

II. THEORY

Within the region of the rarefaction wave, the flow is unsteady and varies spatially, so it cannot be rendered quasisteady by a change of reference frame. Hence we need to establish the governing equations for a *differential* control volume in this region, as shown by the thin gray rectangles in Figs. 2(b) and 2(c), rather than for an integral control volume as in the work of Borden and Meiburg [8,14]. In order to formulate the governing system of equations for this differential control volume, we represent the rarefaction wave as a series of infinitesimal steplike variations in interface height of size dh. A detailed view of this differential control volume is shown in Fig. 3. It contains the section over which the interface height varies from $h - dh/2$ at the left boundary to $h + dh/2$ at

the right boundary, by means of a jump $dh < 0$ at the center of the control volume. The entire control volume moves with the velocity $u(h)$ of the jump. We assume the fluids to be inviscid and their density difference to be sufficiently small for the Boussinesq approximation to be valid. Furthermore, we consider the flow in each layer at the control volume boundaries to be purely horizontal and independent of the vertical coordinate. With this assumption of locally unidirectional flow, we can write the mass conservation equations for the lower and upper layers, i.e., for the control volumes $ABCD$ and $ABEF$, as

$$\left[\left(u_g - \frac{du_g}{2}\right) - u\right]\left(h - \frac{dh}{2}\right) = \left[\left(u_g + \frac{du_g}{2}\right) - u\right]\left(h + \frac{dh}{2}\right), \tag{7}$$

$$\left[\left(u_a + \frac{du_a}{2}\right) + u\right]\left(H - h - \frac{dh}{2}\right) = \left[\left(u_a - \frac{du_a}{2}\right) + u\right]\left(H - h + \frac{dh}{2}\right). \tag{8}$$

By neglecting higher-order terms, Eqs. (7) and (8) simplify to

$$(u_g - u)dh + h du_g = 0, \tag{9}$$

$$(u_a + u)dh - (H - h)du_a = 0. \tag{10}$$

We now derive the conservation equation for the vorticity along the interfacial segment AB within the differential control volume $DCEF$ in Fig. 3. Towards that end, we start from the integral form of the vorticity conservation law for inviscid variable-density flow

$$\frac{d}{dt}\iint_{DCEF(t)} \omega\, dA + \oint_{CS(t)} \omega \mathbf{V}_r \cdot \mathbf{n}\, dS = -\iint_{DCEF(t)} g' \frac{\partial \rho^*}{\partial x}\, dA. \tag{11}$$

Here $CS(t)$ denotes the surface of the control volume $DCEF$ and $\mathbf{V}_r$ represents the velocity of the fluid relative to the moving control volume boundary. The temporal rate of change of the circulation inside the control volume vanishes, because the control volume size and the interface shape within do not change over time

$$\frac{d}{dt}\iint_{DCEF(t)} \omega\, dA = 0. \tag{12}$$

Next, the flux of vorticity crossing the surface of the control volume can be formulated as

$$\begin{aligned}
&\oint_{CS(t)} \omega \mathbf{V}_r \cdot \mathbf{n}\, dS \\
&\quad = -\left[\left(u_a - \frac{du_a}{2}\right) + \left(u_g - \frac{du_g}{2}\right)\right] \times \frac{1}{2}\left[\left(u_g - \frac{du_g}{2}\right) - \left(u_a - \frac{du_a}{2}\right) - 2u\right] \\
&\qquad + \underbrace{\left[\left(u_a + \frac{du_a}{2}\right) + \left(u_g + \frac{du_g}{2}\right)\right]}_{\text{vortex sheet strength}} \times \underbrace{\frac{1}{2}\left[\left(u_g + \frac{du_g}{2}\right) - \left(u_a + \frac{du_a}{2}\right) - 2u\right]}_{\text{vortex sheet principal velocity}}.
\end{aligned} \tag{13}$$

Simplifying Eq. (13) gives

$$\oint_{CS(t)} \omega \mathbf{V}_r \cdot \mathbf{n}\, dS = du_g(u_g - u) - du_a(u_a + u). \tag{14}$$

To evaluate the baroclinic vorticity generation term on the right-hand side of Eq. (11), we remind ourselves that the interface is sharp and that the dimensionless density $\rho^* = 1$ everywhere below the interface and $\rho^* = 0$ everywhere above. Within the control volume $DCEF$, the interface consists of the two horizontal segments to the left and the right and the vertical segment of length dh at the center. Consequently, the only location within the control volume where $\partial\rho^*/\partial x \neq 0$ is along

this vertical interface segment of length dh adjacent to point O. Integration along any horizontal line that crosses this vertical interface segment gives $\int \partial\rho^*/\partial x\, dx = -1$. Consequently, we obtain $\iint \partial\rho^*/\partial x\, dA = -dh$, which results in

$$\iint_{DCEF(t)} g' \frac{\partial \rho^*}{\partial x}\, dA = -g' dh, \tag{15}$$

where $dh < 0$. Since $\partial\rho^*/\partial x \neq 0$ only along the vertical segment of the step, the horizontal interface segments do not contribute to the area integral, so its value is independent of the horizontal extent of the interval $x_r - x_l$. By substituting Eqs. (12), (14), and (15) into (11) we obtain

$$du_g(u - u_g) - du_a(u + u_a) = -g' dh. \tag{16}$$

By combining the continuity equations (9) and (10) with the vorticity equation (16) we obtain the system

$$\frac{du_g}{dh} = -\frac{1}{h}(u_g - u), \tag{17}$$

$$\frac{du_a}{dh} = \frac{1}{H - h}(u_a + u), \tag{18}$$

$$\frac{1}{h/H}(u - u_g)^2 + \frac{1}{1 - h/H}(u + u_a)^2 = g' H. \tag{19}$$

Note that while the dense and light fluid velocities are governed by first-order ordinary differential equations (ODEs), the vorticity equation reduces to an algebraic relationship. We now choose the channel height H and buoyancy velocity $\sqrt{g'H}$ as reference scales to render Eqs. (17)–(19) dimensionless:

$$\frac{du_g^*}{dh^*} = -\frac{1}{h^*}(u_g^* - u^*), \tag{20}$$

$$\frac{du_a^*}{dh^*} = \frac{1}{1 - h^*}(u_a^* + u^*), \tag{21}$$

$$1 = \frac{1}{h^*}(u^* - u_g^*)^2 + \frac{1}{1 - h^*}(u^* + u_a^*)^2, \tag{22}$$

where the asterisk refers to dimensionless variables.

When the rarefaction wave is directly connected to the lock fluid, as shown in Fig. 2(b), both fluids are at rest at the left edge of the rarefaction wave, so

$$u_g^*(H_{\text{lock}}^*) = u_a^*(H_{\text{lock}}^*) = 0. \tag{23}$$

This provides the two required conditions at the left boundary for ODEs (20) and (21). Corresponding boundary conditions for the configuration with the left-propagating bore, shown in Fig. 2(c), will be discussed in Sec. II A. Equation (22) then gives, for the propagation velocity of the left edge of the expansion wave,

$$u_l^* = -u^*(H_{\text{lock}}^*) = \sqrt{H_{\text{lock}}^*(1 - H_{\text{lock}}^*)}. \tag{24}$$

At the right edge O' of the expansion wave, the expansion fan flow has to match the gravity current, so it needs to satisfy

$$u_g^*(h_{g,r}^*) = u_{g,r}^*, \tag{25}$$

$$u_a^*(h_{g,r}^*) = u_{a,r}^*. \tag{26}$$

The gravity current height $h^*_{g,r}$ is determined by the condition

$$h^*_{g,r} = \tfrac{1}{2}(u^*_{g,r} + u^*_{a,r})^2, \tag{27}$$

which arises from the vorticity conservation principle for the gravity current front (cf. [8] and Sec. II of the present paper). Combining (25)–(27) yields the front condition

$$h^*_{g,r} = \tfrac{1}{2}[u^*_g(h^*_{g,r}) + u^*_a(h^*_{g,r})]^2. \tag{28}$$

Then u^*_r can be evaluated by substituting the gravity current properties into the vorticity balance equation (22), which gives

$$u^*_r = (1 - h^*_{g,r})u^*_g(h^*_{g,r}) - h^*_{g,r}u^*_a(h^*_{g,r}) - \sqrt{h^*_{g,r}(1 - h^*_{g,r})\{1 - [u^*_g(h^*_{g,r}) + u^*_a(h^*_{g,r})]^2\}}, \tag{29}$$

where $h^*_{g,r}$ can be calculated from Eq. (28).

The above system of equations (20)–(22), together with the boundary conditions (23) and the front condition (28), thus completely determines the combined expansion fan and gravity current flow. This system can be solved numerically by integrating Eqs. (20) and (21) from H^*_{lock} to the h^* value that satisfies the condition (28). We also update the interfacial velocity u^* from Eq. (22) in each integration step. The interface height at which we terminate the integration process is then the gravity current height. In this study, we employ the standard fourth-order Runge-Kutta scheme to carry out the integration.

Equations (20)–(22) can be recast in terms of a single ODE for $u^*_g(h^*)$. Towards this end, Eqs. (20) and (21) are combined and integrated with respect to h^*, which results in

$$u^*_g h^* = u^*_a(1 - h^*), \tag{30}$$

which simply states that the volume flux to the left above the interface has to equal the volume flux to the right below the interface. We can hence eliminate u^*_a from Eq. (22), so we obtain for u^*, as a function of h^* and u^*_g,

$$u^* = \frac{1 - 2h^*}{1 - h^*}u^*_g \pm \sqrt{\frac{h^*}{1 - h^*}\left[(1 - h^*)^2 - u^{*2}_g\right]}. \tag{31}$$

Substituting Eq. (31) into (20) then yields

$$h^*\frac{du^*_g}{dh^*} + \frac{h^*}{1 - h^*}u^*_g \pm \sqrt{\frac{h^*}{1 - h^*}\left[(1 - h^*)^2 - u^{*2}_g\right]} = 0 \tag{32}$$

for the velocity of the dense fluid within the expansion fan as a function of the local interface height h^*. Interestingly, Eq. (32) is identical to the one obtained by Rottman and Simpson [13] via a two-layer shallow-water analysis, as will be discussed below in further detail.

A. Formation of the left-propagating bore

The earlier investigations by Rottman and Simpson [13] and Shin *et al.* [7] demonstrated that the expansion fan is not always directly connected to the lock fluid, as sketched in Fig. 2(b). Rather, beyond a critical value of the lock height H_{lock} a bore or hydraulic drop forms that connects the left edge of the rarefaction wave to the stationary fluid in the lock, as shown in Fig. 2(c). This is also confirmed by the DNSs to be discussed below. We now proceed to analyze the formation of the bore and its interaction with the left edge of the expansion wave, based on the vorticity approach.

As long as the interfacial wave speed u^* varies monotonically with h^* throughout the expansion fan region, the slope of the fan's interface will decrease everywhere with time, so a bore does not form. If, on the other hand, u^* reaches an extremum u^*_{min} for an intermediate value of h^*, the interfacial segment with this minimum velocity travels leftward faster than the left edge of the wave and catches up with it. The interface hence steepens locally and a bore forms where the expansion fan meets the lock fluid, as sketched in Fig. 2(c). This situation corresponds to the observation by

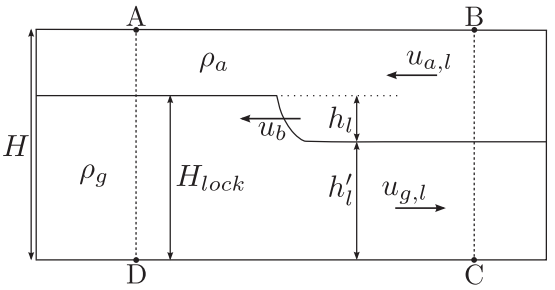

FIG. 4. Schematic of the control volume around the hydraulic drop of the configuration in Fig. 2(c).

Rottman and Simpson [13] of a multivalued solution for the interfacial height when $H^*_{\text{lock}} > 0.5$. Now the boundary conditions at the left edge of the expansion fan take the form

$$u^*_g(h'^*_l) = u^*_{g,l}, \tag{33}$$

$$u^*_a(h'^*_l) = u^*_{a,l}. \tag{34}$$

In order to determine the value of H^*_{lock} at which the bore first appears, we need to determine the value of H^*_{lock} for which the u^* profile first exhibits an extremum. Taking the derivative of Eq. (22) with respect to h^* yields

$$\left(\frac{2(u^* - u^*_g)}{h^*} + \frac{2(u^* + u^*_a)}{1 - h^*}\right)\frac{du^*}{dh^*} - \frac{3(u^* - u^*_g)^2}{h^{*2}} + \frac{3(u^* + u^*_a)^2}{(1 - h^*)^2} = 0, \tag{35}$$

where du^*_g/dh^* and du^*_a/dh^* have been replaced based on Eqs. (20) and (21). A local minimum for the interfacial velocity ($du^*/dh^* = 0$) exists when

$$\frac{u^* - u^*_g}{h^*} = \frac{u^* + u^*_a}{1 - h^*}. \tag{36}$$

As we will see in Sec. II B, a u^* minimum first appears for the largest value of h^*, i.e., at the left edge of the rarefaction wave [location O in Fig. 2(b)] where $u^*_g = u^*_a = 0$. For these conditions, Eq. (36) gives $H^*_{\text{lock}} = 0.5$, which agrees with the findings of Rottman and Simpson [13].

For flows with bores we have to match the left edge of the expansion fan to the bore at the interface height h'_l [cf. Fig. 2(c)]. To obtain the velocities of the upper and lower fluid layers between the bore and the expansion fan, we first investigate the left-propagating bore in isolation from the rest of the flow, as sketched in Fig. 4. In the reference frame moving with the bore, the continuity equations for both layers and the vorticity conservation equation for the control volume $ABCD$ in Fig. 4 read

$$u^*_b H^*_{\text{lock}} = (u^*_b + u^*_{g,l})h'^*_l, \tag{37}$$

$$u^*_b(1 - H^*_{\text{lock}}) = (u^*_b - u^*_{a,l})(1 - h'^*_l), \tag{38}$$

$$\tfrac{1}{2}(u^*_{g,l} + u^*_{a,l})(2u^*_b + u^*_{a,l} - u^*_{g,l}) = h^*_l \tag{39}$$

(cf. [14]). If the interface height h'_l to the right of the bore is known, these equations fully determine the fluid and bore velocities. In order to understand how the flow selects this interface height, it is instructive to analyze the energetics of the bore region. Towards this end, we determine the pressure difference along the top wall $p_A - p_B$ from the horizontal momentum conservation equation for

$ABCD$,

$$\int_D^A [\rho_{\text{ref}} u_i(y)^2 + p_i(y)]dy = \int_C^B [\rho_{\text{ref}} u_o(y)^2 + p_o(y)]dy, \tag{40}$$

where $p_i(y)$ and $p_o(y)$ indicate the pressure functions from A to D and B to C, respectively, and $u_i(y)$ and $u_o(y)$ represent the piecewise constant fluid velocities across the in- and outflow boundaries, respectively. The reference density is also $\rho_{\text{ref}} = \rho_a$. The pressure can be considered hydrostatic far up- and downstream of the bore, so $p_i(y)$ and $p_o(y)$ take the forms

$$p_i(y) = \begin{cases} p_A + \rho_a g(H - y), & y \geqslant H_{\text{lock}} \\ p_A + \rho_a g(H - H_{\text{lock}}) + \rho_g g(H_{\text{lock}} - y), & y < H_{\text{lock}}, \end{cases} \tag{41}$$

$$p_o(y) = \begin{cases} p_B + \rho_a g(H - y), & y \geqslant h_l' \\ p_B + \rho_a g(H - h_l') + \rho_g g(h_l' - y), & y < h_l'. \end{cases} \tag{42}$$

Nondimensionalizing these relations and substituting them into Eq. (40) yields

$$p_A^* - p_B^* = h_l'^*(u_b^* + u_{g,l}^*)^2 + (1 - h_l'^*)(u_b^* - u_{a,l}^*)^2 - u_b^{*2} - \tfrac{1}{2}\left(H_{\text{lock}}^{*\,2} - h_l'^{*2}\right), \tag{43}$$

where the dimensional pressures have been divided by $\rho_a g' H$ to obtain the dimensionless ones. The rate of dissipation of energy ΔE for the entire control volume, in the reference frame of the bore, can be calculated as

$$\Delta \dot{E} = \int_D^A \left(\frac{1}{2}\rho_a u_i^2 + p_i + \rho_i g y\right) u_i dy - \int_C^B \left(\frac{1}{2}\rho_a u_i^2 + p_o + \rho_o g y\right) u_o dy, \tag{44}$$

where ρ_i and ρ_o denote the fluid densities at the in- and outlet of $ABCD$, respectively. After nondimensionalization and simplification, Eq. (44) reads

$$\begin{aligned} \Delta \dot{E}^* = {} & (p_A^* - p_B^*)u_b^* + H_{\text{lock}}^*(H_{\text{lock}}^* - h_l'^*)u_b^* + \tfrac{1}{2}u_b^{*3} - \tfrac{1}{2}h_l'^*(u_b^* + u_{g,l}^*)^3 \\ & - \tfrac{1}{2}(1 - h_l'^*)(u_b^* - u_{a,l}^*)^3. \end{aligned} \tag{45}$$

Note that $\Delta \dot{E}$ has been scaled by $\rho_a g'^{3/2} H^{5/2}$ to be rendered dimensionless.

Figure 5 displays the net rate of energy loss $\Delta \dot{E}$ for the bore sketched in Fig. 4, as a function of $h_l'^*$ and for several values of H_{lock}^*. The results show that, independent of the lock height, the interface height $h_l'^* = 0.5$ corresponds to energy-conserving flow. An interface height of less than half the channel height would require an energy gain, so it cannot be physically realized. As we will see in the DNSs to be discussed below, for all lock heights the flow develops a nearly-energy-conserving bore with an interface height $h_l'^* \approx 0.5$, corresponding to the familiar observation of an energy-conserving half-depth current for a full-depth lock release [6,8].

Substituting $h_l'^* = 0.5$ into Eqs. (37)–(39) then gives $u_b^* = 0.5$ and $u_{g,l}^* = u_{a,l}^* = H_{\text{lock}}^* - 0.5$. In Sec. IV we will compare these results to DNS simulations. These flow velocities $u_{g,l}^*$ and $u_{a,l}^*$ to the right of the bore can now serve as boundary conditions at the left edge of the expansion fan. Substitution into Eq. (22) yields the propagation velocity of the left edge of the rarefaction wave

$$u_l^* = \sqrt{H_{\text{lock}}^*(1 - H_{\text{lock}}^*)}. \tag{46}$$

This result is identical to Eq. (24), which represents the velocity of left edge of the expansion fan for the configuration in Fig. 2(b) without a bore. For any lock height $H_{\text{lock}}^* > 0.5$, we can now solve Eqs. (20)–(22) in the interval $h_{g,r}^* \leqslant h^* \leqslant h_l'^* = 0.5$, subject to these boundary conditions and the front condition (28).

B. Predictions by the vorticity-based model

We employ a standard fourth-order Runge-Kutta method to solve Eqs. (20) and (21), along with the algebraic equation (22), for the configuration sketched in Fig. 2(b). For now, we apply boundary

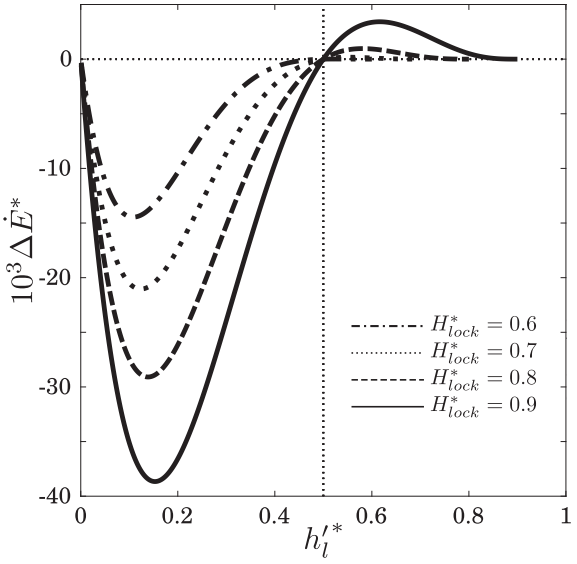

FIG. 5. Variation of the rate of dissipation of energy $\Delta\dot{E}^*$ as a function of the interface height after the hydraulic drop $h_l'^*$, computed for an isolated bore traveling along the interface of a two-layer flow for various lock heights H^*_{lock}. For all lock heights, an interface height $h_l'^* = 0.5$ after the bore corresponds to energy-conserving flow.

conditions (23) at $h^* = H^*_{\text{lock}}$ and the condition (28) at the front. The validity of the conditions (23) will then have to be established *a posteriori*, based on whether or not they result in a multivalued solution, as discussed in Sec. II A. Figure 6(a) displays the dense and light fluid velocities as functions of the local interface height for the specific lock height value $H^*_{\text{lock}} = 0.5$. The lower layer fluid continually speeds up from the lock towards the gravity current, while the upper layer velocity is seen to reach a local maximum close to where the expansion fan transitions to the gravity current.

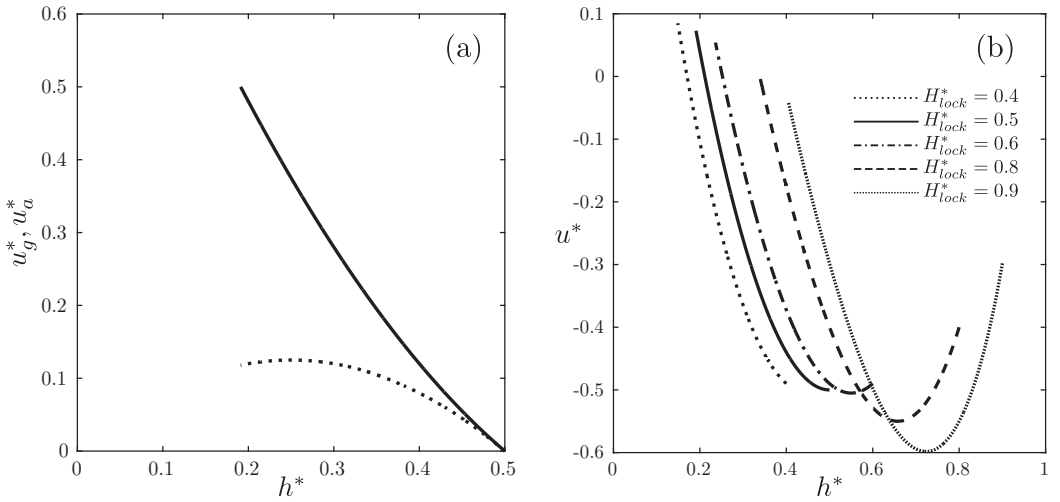

FIG. 6. (a) Variation of the lower layer velocity u_g^* (solid line) and the upper layer velocity u_a^* (dotted line), as a function of the local interface height h^*, for $H^*_{\text{lock}} = 0.5$. (b) Interfacial velocity u^* as a function of h^* along the rarefaction wave, for various values of the lock height H^*_{lock}. These solutions were obtained based on the configuration in Fig. 2(b), with boundary conditions (23).

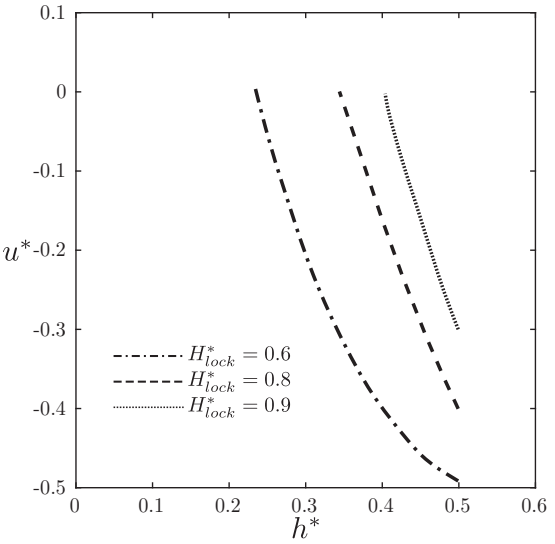

FIG. 7. Variation of the interfacial velocity u^* as a function of h^* along the expansion fan, for various values of $H^*_{\text{lock}} > 0.5$. These solutions were obtained based on the configuration in Fig. 2(c) and boundary conditions (33) and (34). As discussed in the text, in these cases the left edge of the rarefaction wave is located at $h^* = h_l^* = 0.5$ and the solution for u^* exists only for the range $h^*_{g,r} \leqslant h^* \leqslant 0.5$.

Figure 6(b) shows the interfacial velocity u^* as a function of the interface height h^* for several different lock heights. As we anticipated based on the analysis in Sec. II A, for $H^*_{\text{lock}} = 0.4$ and 0.5 the interfacial velocity u^* increases monotonically from negative values at the lock to positive values in the vicinity of the gravity current, which indicates that the left edge of the expansion fan travels to the left, while its right edge travels to the right. For $H^*_{\text{lock}} = 0.6$, 0.8, and 0.9, on the other hand, we find that solutions based on the configuration shown in Fig. 2(b), with boundary conditions (23), yield a local minimum for an intermediate interface height near the lock, which indicates that a left-propagating bore will form, so that boundary conditions (23) are invalid, and interfacial velocities below -0.5 will not emerge in the flow. Figure 6(b) confirms that a bore first appears for $H^*_{\text{lock}} = 0.5$, since for this value the slope of $u^*(h^*)$ first vanishes at the left edge of the expansion fan. These results are consistent with the analysis of Sec. II A and with the findings of Rottman and Simpson [13].

The analysis in Sec. II A, along with the observations of multivalued solutions for the interfacial velocity when $H^*_{\text{lock}} > 0.5$, suggests that in this regime boundary conditions (33) and (34) need to be enforced, which results in the interfacial velocities shown in Fig. 7. Now u^* decreases monotonically with h^* and the expansion fan is confined to the range $h^*_{g,r} \leqslant h^* \leqslant 0.5$.

C. Relationship between the vorticity-based model and the two-layer shallow-water equations

Rottman and Simpson [13] derive Eq. (32) from the two-layer shallow-water equations, after employing the method of characteristics. In the following, we will show that in the limit of locally unidirectional flow and when the velocity does not vary across the thickness of each layer, the vorticity model is consistent with the shallow-water equations. This discussion is merely intended to clarify the relationship between the two approaches and to establish under what conditions they are equivalent to each other. The two-layer shallow water equations have clearly proved to be highly useful and we do not mean to imply any shortcomings of this approach.

Figure 8 displays an arbitrary two-layer stratified flow, with the gray rectangular area indicating a fixed control volume of length Δx. For a two-dimensional inviscid flow in the Boussinesq

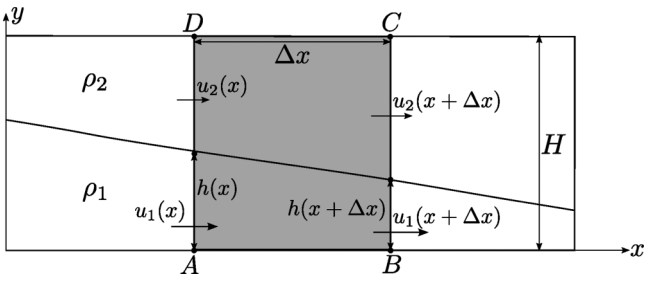

FIG. 8. Control volume employed for the purpose of discussing the relationship between the vorticity-based model and the shallow water equations (see the discussion in the text).

approximation, the vorticity equation reads

$$\frac{\partial \omega}{\partial t} + \mathbf{u} \cdot \nabla \omega = -g' \frac{\partial \rho^*}{\partial x}. \tag{47}$$

Integration over control volume $ABCD$ yields

$$\underbrace{\iint_{ABCD} \frac{\partial \omega}{\partial t} dA}_{I_1} + \underbrace{\oint_{CS} \omega \mathbf{u} \cdot \mathbf{n}\, dS}_{I_2} = \underbrace{\iint_{ABCD} -g' \frac{\partial \rho^*}{\partial x} dA}_{I_3}, \tag{48}$$

where CS denotes the surface of the control volume $ABCD$. We now consider the flow to be locally unidirectional at the in- and outflow boundaries and assume that u_1 and u_2 do not vary with y. The integrals in Eq. (49) can then be evaluated individually. Integral I_1, which accounts for the temporal rate of change of vorticity within $ABCD$, yields

$$I_1 = \frac{\partial}{\partial t} \int_x^{x+\Delta x} dx \int_0^H -\frac{\partial u}{\partial y} dy = \frac{\partial}{\partial t} \int_x^{x+\Delta x} -(u_2 - u_1) dx. \tag{49}$$

Here I_2 accounts for the convective flux of vorticity into and out of the control volume, which can be obtained by multiplying the strength of the vortex sheet with its principal velocity. Consequently,

$$I_2 = \frac{u_1^2(x+\Delta x) - u_1^2(x)}{2} - \frac{u_2^2(x+\Delta x) - u_2^2(x)}{2}. \tag{50}$$

Finally, the baroclinic vorticity generation can be evaluated as

$$\begin{aligned} I_3 &= \int_0^H dy \int_x^{x+\Delta x} -g' \frac{\partial \rho^*}{\partial x} dx = \int_0^H -g'[\rho^*(x+\Delta x) - \rho^*(x)] dy \\ &= -g'[h(x+\Delta x) - h(x)]. \end{aligned} \tag{51}$$

In the limit of $\Delta x \to 0$, we thus obtain

$$\frac{\partial u_2}{\partial t} - \frac{\partial u_1}{\partial t} + u_2 \frac{\partial u_2}{\partial x} - u_1 \frac{\partial u_1}{\partial x} = g' \frac{\partial h}{\partial x}. \tag{52}$$

This is identical to what one obtains in the Boussinesq limit from the shallow-water equations when subtracting the lower layer momentum equation (3.3) from the upper layer one (3.4) in [13]. We thus conclude that, perhaps not unexpectedly, for locally unidirectional flow with constant velocity across the height of each layer, the vorticity-based model and shallow-water theory are equivalent to each other. When the velocity is not approximately unidirectional, such as in the vicinity of a gravity current front or an internal bore, shallow-water theory is no longer applicable, whereas vorticity-based models are still able to capture the physics correctly.

III. THE DNS RESULTS

In the following, we compare predictions by the vorticity model with DNS results, as well as with earlier experimental data and model predictions by other authors. The DNS data were obtained with our code TURBINS, which has been described and validated in detail by Nasr-Azadani and Meiburg [15,16]. TURBINS is a finite-difference solver based on a fractional step projection method, along with total variation diminishing Runge-Kutta time integration. It solves the unsteady, incompressible Navier-Stokes equations in the Boussinesq limit

$$\nabla \cdot \mathbf{V}^* = 0, \tag{53}$$

$$\frac{\partial \mathbf{V}^*}{\partial t^*} + \mathbf{V}^* \cdot \nabla \mathbf{V}^* = -\nabla p^* + \frac{1}{\mathrm{Re}} \nabla^2 \mathbf{V}^* + \rho^* \mathbf{e}^g, \tag{54}$$

$$\frac{\partial \rho^*}{\partial t^*} + \mathbf{V}^* \cdot \nabla \rho^* = \frac{1}{\mathrm{Pe}} \nabla^2 \rho^*, \tag{55}$$

where $\mathbf{V}^*$ and $\mathbf{e}^g$ represent the velocity vector and unit vector in the direction of gravity, respectively. The dimensionless time is defined as $t^* = t/\sqrt{H/g'}$. The governing dimensionless parameters have the form of a Reynolds number $\mathrm{Re} = \sqrt{g' H_{\mathrm{lock}}} H_{\mathrm{lock}}/\nu$ and a Péclet number $\mathrm{Pe} = \sqrt{g' H_{\mathrm{lock}}} H_{\mathrm{lock}}/D$. Here ν indicates the kinematic viscosity and D denotes the diffusivity of the density field. We apply free-slip conditions for the velocity, along with vanishing normal flux conditions for the density field, along all solid boundaries. Re and Pe are set to 8000 and 40 000 in the simulations, respectively, to minimize the effects of diffusion. Initially the fluids are at rest and the density field is as sketched in Fig. 2(a). The computational domain has the dimensionless size 70×1 and the lock length is set to 35. The domain is discretized uniformly with $\Delta x^* = 0.01$ and $\Delta y^* = 0.004$, which is sufficiently fine to yield converged results.

Figure 9 shows the temporal evolution of a partial lock-release flow for various values of the lock height H^*_{lock}. All values of H^*_{lock} give rise to a right-propagating gravity current ahead of a rarefaction wave. On the other hand, the left-propagating flow varies qualitatively with H^*_{lock}. For small values of H^*_{lock}, the rarefaction wave extends all the way to the lock fluid. For increasing lock heights, the front propagating into the lock fluid becomes steeper and borelike, as can be seen in Figs. 9(e) and 9(f). This observation is consistent with the earlier investigations of Rottman and Simpson [13] and Shin *et al.* [7]. Rottman and Simpson [13] state that this bore begins to form experimentally when $H^*_{\mathrm{lock}} \approx 0.7$, while their model predicts bore formation for $H^*_{\mathrm{lock}} > 0.5$, in agreement with our analysis in Sec. II. They attribute this discrepancy to diffusive effects and interfacial mixing, both of which are neglected in their theory. Shin *et al.* [7] argue that the formation of the left-propagating bore starts when infinitesimal long waves travel faster than the left edge of the rarefaction wave, which is theoretically shown to occur for $H^*_{\mathrm{lock}} > 2/3$.

To evaluate the front velocity of the gravity current in the DNS, we track its front location $x^*_{g,r}$ with time. We define the local dimensionless interface height $\eta^*(x^*,t^*)$ as

$$\eta^*(x^*,t^*) = \int_0^1 \rho^*(x^*,y^*,t^*) dy^* \tag{56}$$

and determine $x^*_{g,r}$ as the rightmost location at which $\eta^* > 0.01$. The solid lines in Figs. 10(a) and 11(a) show that for $H^*_{\mathrm{lock}} = 0.5$ and 0.8 the slope $dx^*_{g,r}/dt^*$ becomes constant after a brief initial transient, which indicates a quasisteady gravity current velocity.

Finding the horizontal location of the right edge x^*_r of the rarefaction wave as a function of time is slightly more complicated. Figure 12 shows that behind the gravity current head the interface height drops abruptly. For $H^*_{\mathrm{lock}} \leqslant 0.5$, an extended interface segment of nearly constant height follows that can easily be identified. For $H^*_{\mathrm{lock}} > 0.5$, on the other hand, the gravity current exhibits significant turbulence, so its interface height fluctuates until it reaches the rarefaction wave. Within the rarefaction wave region, the interface height fluctuations are much reduced. Consequently, in order to identify x^*_r coming from the left, we search for the end of an extended region of at least

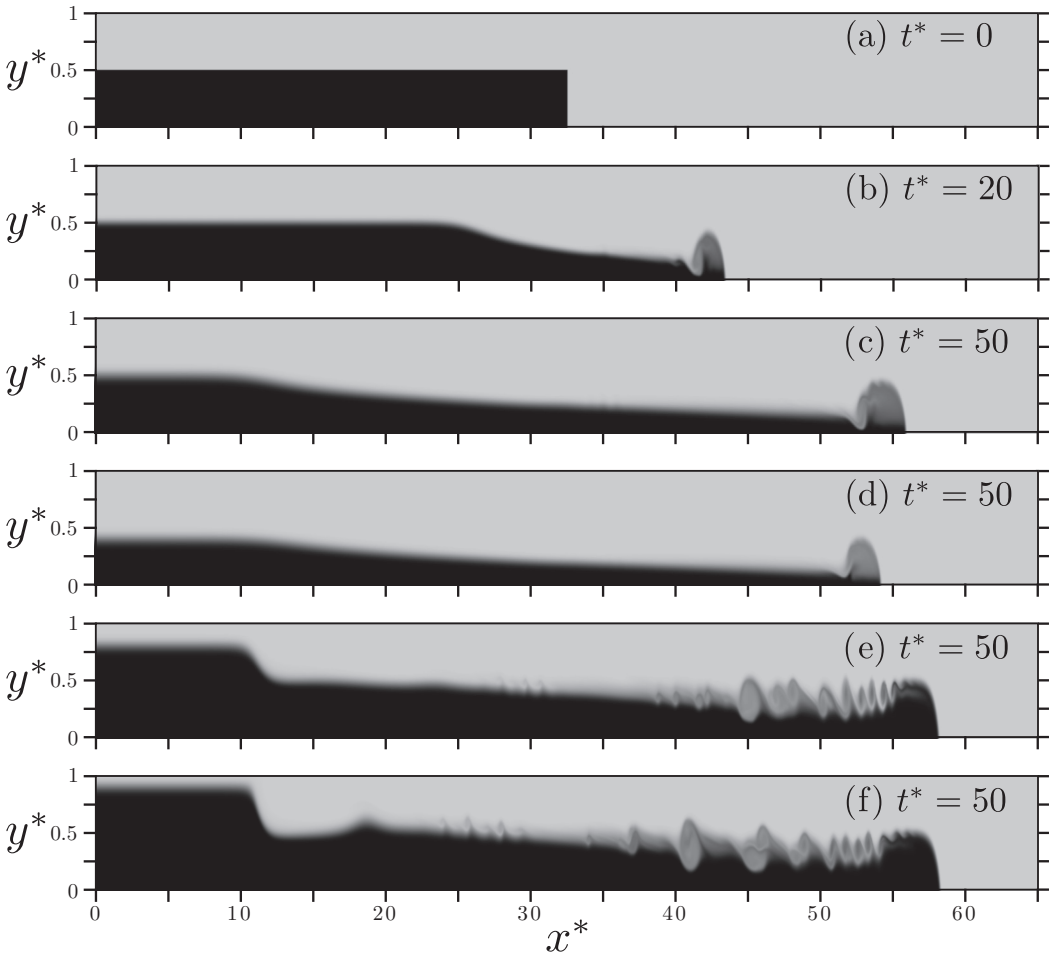

FIG. 9. (a)–(c) Temporal evolution of the density field for a partial-depth lock-release flow with $H^*_{\text{lock}} = 0.5$. (d)–(f) Density field at $t^* = 50$ for (d) $H^*_{\text{lock}} = 0.4$, (e) $H^*_{\text{lock}} = 0.8$, and (f) $H^*_{\text{lock}} = 0.9$. The density field varies from $\rho^* = 0$ (light gray) to $\rho^* = 1$.

three unit lengths over which $\partial\eta^*/\partial x^*$ does not change its sign. The data shown by the dotted lines in Figs. 10(a) and 11(a) indicate that this methodology is successful in identifying the right edge of the expansion fan and finding its propagation velocity, which is constant to a good approximation. We note that for $H^*_{\text{lock}} = 0.8$ the velocity of the right edge u^*_r is substantially smaller as compared to $H^*_{\text{lock}} = 0.5$. These DNS data will be compared to model predictions in Sec. IV.

After determining the locations of the gravity current front $x^*_{g,r}$ and the right edge of the rarefaction wave x^*_r, the gravity current height $h^*_{g,r}$ can be obtained as the average of η^* over the interval from x^*_r to $x^*_{g,r}$,

$$h^*_{g,r} = \frac{\int_{x^*_r}^{x^*_{g,r}} \eta^*(x^*, t^*_s)\, dx^*}{x^*_{g,r} - x^*_r}, \tag{57}$$

where t^*_s should be chosen sufficiently large such that the gravity current height has become time independent. Here we take $t^*_s = 50$.

The left edge of the rarefaction wave is the location at which the interface height begins to decrease from its lock value H^*_{lock}. Hence, its location x^*_l can be obtained as the leftmost point for

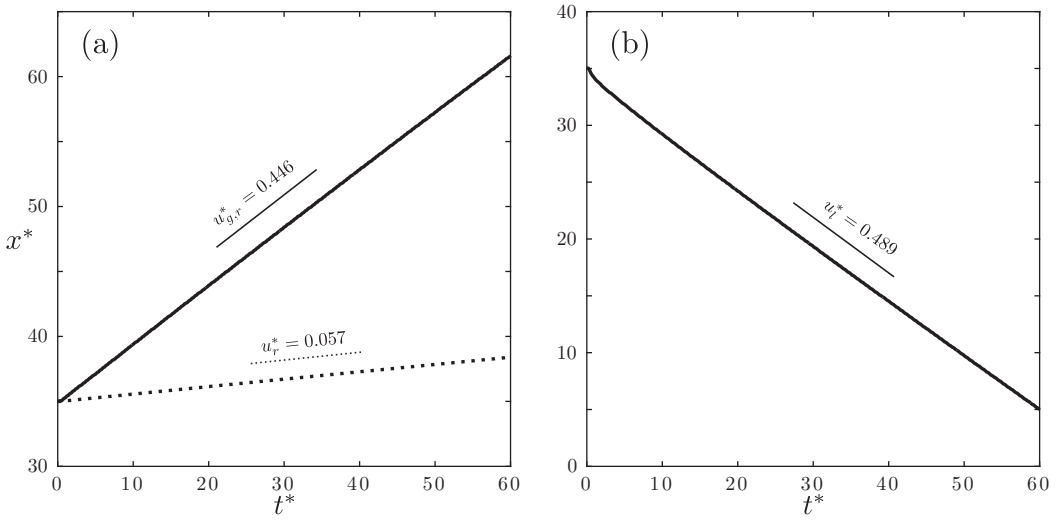

FIG. 10. Plot of the DNS results for the temporal evolution of (a) the front location of the gravity current (solid line) and the location of the right edge of the rarefaction wave (dotted line) and (b) the location of the left edge of the wave, for $H^*_{\text{lock}} = 0.5$. The straight line segments represent the corresponding quasisteady velocities, obtained by linear fits of the DNS results.

which $|\eta^* - H^*_{\text{lock}}| > 0.01$. For $H^*_{\text{lock}} > 0.5$, when the flow gives rise to the left-propagating bore, this procedure yields the horizontal location of the left edge of the bore, denoted by x^*_b. In the presence of a bore, the left edge of the expansion fan x^*_l is found as follows. Coming from the bore, we look for the first location where $|\partial\eta^*/\partial x^*| < 0.01$ to make sure we have exited the bore region. We refer to this point as x^*_e. We then identify the left edge of the rarefaction wave x^*_l as the first

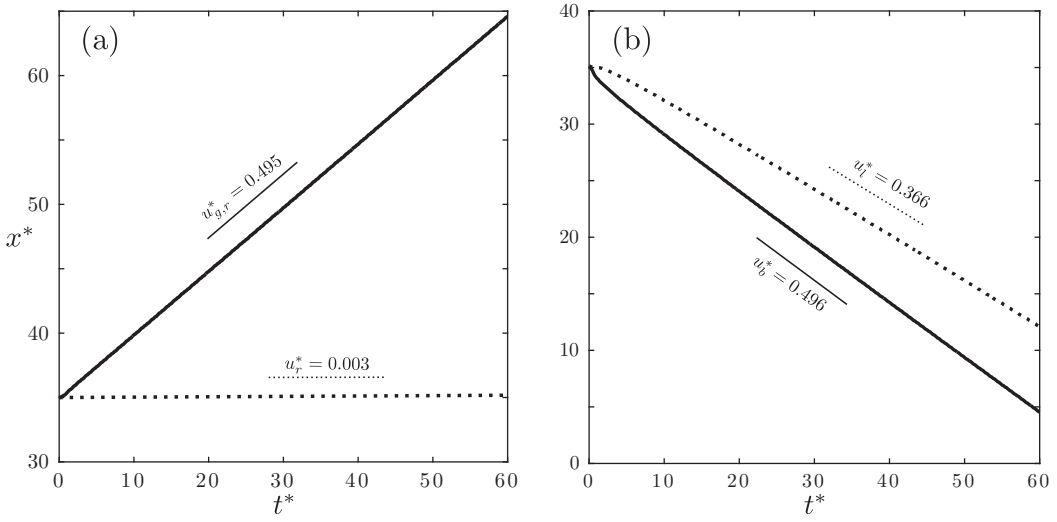

FIG. 11. Plot of the DNS results for the temporal evolution of (a) the front location of the gravity current (solid line) and the location of the right edge of the rarefaction wave (dotted line) and (b) the left edge of the bore (solid line) and of the rarefaction wave (dotted line), for $H^*_{\text{lock}} = 0.8$. The straight line segments represent the corresponding quasisteady velocities, obtained by linear fits of the DNS results.

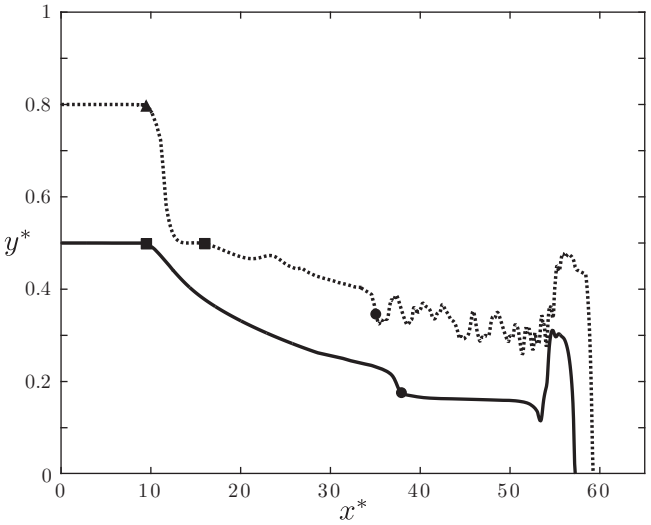

FIG. 12. Plot of the DNS results for the local interface height at $t^* = 50$, for $H^*_{\text{lock}} = 0.5$ (solid line) and 0.8 (dotted line). The circles, squares, and the triangle represent the locations of the right and left edges of the rarefaction wave, as well as the left edge of the bore.

location where $|\partial\eta^*/\partial x^*|$ exceeds 0.01 again. The interface height right after the hydraulic drop can then be calculated in the same fashion as the gravity current height, i.e., by averaging the local interface height η^* from x^*_e to x^*_l,

$$h'^*_l = \frac{\int_{x^*_e}^{x^*_l} \eta^*(x^*, t^*_s)dx^*}{x^*_l - x^*_e}. \tag{58}$$

Again, we select $t^*_s = 50$, which yields a quasisteady result.

Figures 10(b) and 11(b) represent the temporal variation of x^*_l and x^*_b for $H^*_{\text{lock}} = 0.5$ and 0.8, respectively. Note that the case $H^*_{\text{lock}} = 0.5$ is just at the limit of the regime where a left-propagating bore begins to form. After a brief initial transient, x^*_l and x^*_b vary linearly with time, indicating that the bore and the left edge of the expansion wave travel with constant velocities. The bore velocity is seen to be very close to 0.5, which is consistent with the analysis in Sec. II A. Additionally, in agreement with the findings of Sec. II A, Fig. 11(b) confirms that the left edge of the rarefaction wave travels more slowly than the bore, so the distance between the bore and the expansion fan grows with time.

IV. THE DNS COMPARISONS

Figure 13 compares the predictions by the differential vorticity model with DNS results, as well as with earlier model predictions and experimental data by other authors where available. All existing models predict a continuous increase of the gravity current height with the lock height. The experimental and DNS results generally fall in between the various model predictions and indicate a gravity current height slightly less than half the lock height. Both the results of Shin *et al*. [7] and the vorticity model recover the classical full-depth lock-exchange result of Benjamin [6] and Borden and Meiburg [8]. Equations (24) and (29) of the present model also correctly predict that $u^*_l = u^*_r = 0$ in this limit, indicating that no expansion fan forms for a full-depth lock release. The model of Rottman and Simpson [13] does not converge to this limit, as it does not account for the left-propagating bore. Regarding the gravity current velocity, Shin *et al*. [7] predict a continuous increase with lock height, whereas the vorticity model yields a maximum value of $u^*_{g,r}$ for $H^*_{\text{lock}} = 0.789$, which corresponds to $h^*_{g,r} = 0.333$. This is consistent with the analysis of Borden and Meiburg [8] and close to the results

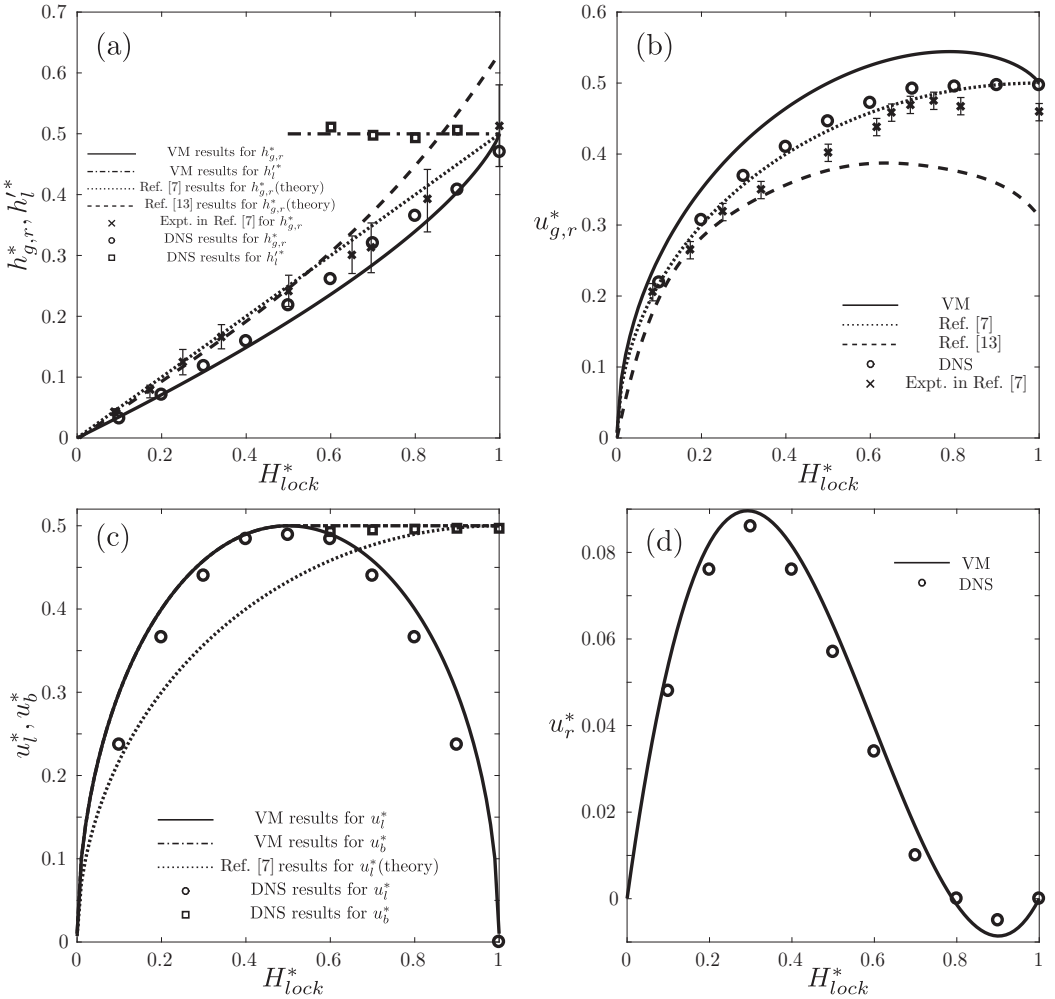

FIG. 13. Variation as a function of the lock height H^*_{lock}: (a) the height $h^*_{g,r}$ of the gravity current and the interface height $h_l'^*$ after the hydraulic drop, (b) the velocity $u^*_{g,r}$ of the gravity current, (c) the velocity u^*_l of the left edge of the rarefaction wave and the velocity u^*_b of the bore, and (d) the velocity u^*_r of the right edge of the rarefaction wave. Here VM refers to the current vorticity-based model.

of Benjamin [6], which display a maximum at $h^*_{g,r} = 0.347$. Although the gravity current speeds predicted by Shin *et al*. [7] agree more closely with the DNS and experimental results compared to those of the present study and Rottman and Simpson [13], we should note that unlike other models, Shin *et al*. [7] cannot obtain $u^*_{g,r}$ for a gravity current with a given height, unless the height of the lock from which this gravity current has been produced is also prescribed, as can be realized from Eq. (6).

The DNS data for u^*_b are consistent with the finding by the vorticity model that a left-propagating bore emerges when the lock height exceeds half the tank depth and that this bore travels with a velocity of 0.5, independent of H^*_{lock}. The current model also predicts that the interface height after this hydraulic drop $h_l'^*$ is always equal to 0.5, in very close agreement with DNS results. In addition, the vorticity model predicts, and the DNS results confirm, that the dependence of the expansion fan's left edge velocity u^*_l on H^*_{lock} is symmetric with regard to $H^*_{\text{lock}} = 0.5$. The model of Shin *et al*. [7], on the other hand, predicts that the propagation speed of the fastest leftward disturbance, as represented by the left edge of the expansion fan before the formation of the bore and the bore

otherwise, is always opposite and equal to the gravity current velocity, which is not confirmed by the current DNS results. The vorticity model predictions for u_r^*, which are in close agreement with the DNS results, become negative beyond $H_{\text{lock}}^* = 0.789$, so the rarefaction wave as a whole travels to the left.

V. ENERGY ASSESSMENT

When deriving the set of governing equations, we did not invoke any assumptions about energy conservation or energy losses in the flow. Consequently, we can now assess the energetics of the flow *a posteriori*, by evaluating the head loss along the top wall of the tank from B to A in Figs. 2(b) and 2(c). The pressure difference along this streamline can be calculated from the horizontal momentum balance for the control volume $ABDE$ in the laboratory reference frame. The flow is at rest at AE and BD and the velocity along the top wall is taken from the preceding analysis. Due to the unsteadiness of the flow within $ABDE$, we need to employ the unsteady form of the streamwise momentum conservation equation and account for the rate $\dot{M}$ at which momentum changes within the control volume. Hence, we obtain

$$\dot{M} = \int_D^B p\, dy - \int_E^A p\, dy = (p_B - p_A)H - (\rho_g - \rho_a)g\frac{H_{\text{lock}}^2}{2}, \tag{59}$$

where we assume that the pressure is hydrostatic at the boundaries. The rate at which momentum inside $ABDE$ changes with time is given by the sum of the rates at which momentum changes inside the gravity current, expansion wave, and left-propagating bore regions

$$\dot{M} = \dot{M}_{gc} + \dot{M}_w + \dot{M}_{lb}. \tag{60}$$

These individual rates can be calculated by multiplying the rate at which the area of the flow region under consideration increases, with the momentum per unit area. Consequently,

$$\dot{M}_{gc} = \rho_a(u_{g,r} - u_r)[u_{g,r}h_{g,r} - u_{a,r}(H - h_{g,r})], \tag{61}$$

$$\dot{M}_w = \int_{h_{g,r}}^{H_{\text{lock}}} \rho_a \frac{du}{dh}[u_g h - u_a(H - h)]dh, \tag{62}$$

$$\dot{M}_{lb} = \rho_a(u_b - u_l)[u_{g,l}h_l' - u_{a,l}(H - h_l')]. \tag{63}$$

Mass conservation gives $u_{g,r}h_{g,r} = u_{a,r}(H - h_{g,r})$ for the gravity current, $u_g h = u_a(H - h)$ in the expansion wave, and $u_{g,l}h_l' = u_{a,l}(H - h_l')$ for the bore, so the right-hand sides of Eqs. (61)–(63) vanish in the Boussinesq limit. Hence we obtain $\dot{M} = 0$, so Eq. (59) yields

$$p_B - p_A = (\rho_g - \rho_a)g\frac{H_{\text{lock}}^2}{2H}. \tag{64}$$

Once we determine the pressure difference $p_B - p_A$ along the top wall, the corresponding head loss Δ can then be obtained from the unsteady form of Bernoulli's equation along streamline BA,

$$p_B + \frac{1}{2}\rho_a u_B^2 + \rho_a \frac{\partial \phi}{\partial t}\bigg|_B = p_A + \frac{1}{2}\rho_a u_A^2 + \rho_a \frac{\partial \phi}{\partial t}\bigg|_A + \Delta. \tag{65}$$

Here ϕ denotes the velocity potential for the upper layer. In addition, u_A and u_B represent the flow velocities at A and B, which vanish as the fluid is at rest at these locations. Clearly, ϕ has to be continuous and its x derivative should recover the horizontal velocity in the ambient. These

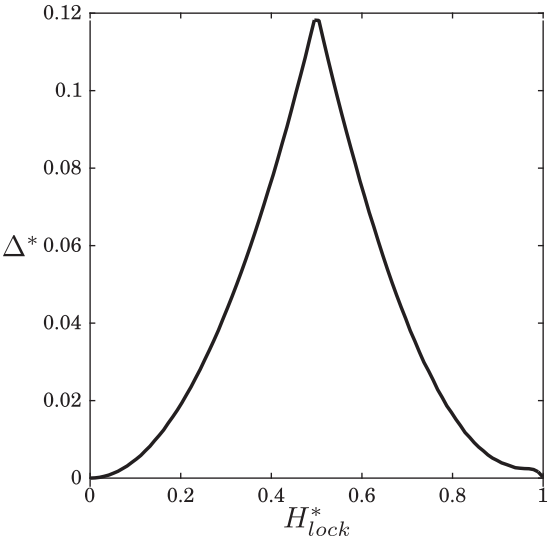

FIG. 14. Head loss Δ^* along the top wall of the tank, computed from B to A, as a function of the lock height H^*_{lock}.

conditions can be satisfied for $H_{\text{lock}} \leqslant H/2$ by

$$\phi = \begin{cases} 0 & \text{for } x_A \leqslant x < x_O \\ -\int_{x_O}^{x} u_a ds & \text{for } x_O \leqslant x < x_{O'} \\ -u_{a,r}(x - x_{O'}) - \int_{x_O}^{x_{O'}} u_a ds & \text{for } x_{O'} \leqslant x < x_F \\ -u_{a,r}(x_F - x_{O'}) - \int_{x_O}^{x_{O'}} u_a ds & \text{for } x_F \leqslant x \leqslant x_B \end{cases} \tag{66}$$

and for $H_{\text{lock}} > H/2$ by

$$\phi = \begin{cases} 0 & \text{for } x_A \leqslant x < x_C \\ -u_{a,l}(x - x_C) & \text{for } x_C \leqslant x < x_O \\ -u_{a,l}(x_O - x_C) - \int_{x_O}^{x} u_a ds & \text{for } x_O \leqslant x < x_{O'} \\ -u_{a,r}(x - x_{O'}) - u_{a,l}(x_O - x_C) - \int_{x_O}^{x_{O'}} u_a ds & \text{for } x_{O'} \leqslant x < x_F \\ -u_{a,r}(x_F - x_{O'}) - u_{a,l}(x_O - x_C) - \int_{x_O}^{x_{O'}} u_a ds & \text{for } x_F \leqslant x \leqslant x_B. \end{cases} \tag{67}$$

Relation (66) or (67) can be substituted into Eq. (65) to obtain Δ. We render the result dimensionless by scaling pressure and head loss with $p_{\text{ref}} = \Delta_{\text{ref}} = \rho_a g' H$. The other variables are nondimensionalized as described in Sec. II. We thus obtain, for the dimensionless heaadloss Δ^*,

$$\Delta^* = \begin{cases} {H^*_{\text{lock}}}^2/2 - u^*_{a,r} u^*_{g,r} + \int_{h^*_{g,r}}^{H^*_{\text{lock}}} \frac{du^*_a}{dh^*} u^* dh^* & \text{for } H^*_{\text{lock}} \leqslant 0.5 \\ {H^*_{\text{lock}}}^2/2 - u^*_{a,r} u^*_{g,r} - u^*_{a,l} u^*_b + \int_{h^*_{g,r}}^{h^{l*}_l} \frac{du^*_a}{dh^*} u^* dh^* & \text{otherwise.} \end{cases} \tag{68}$$

Figure 14 displays the head loss along the top wall for the entire range of H^*_{lock}. Consistent with the analyses of Benjamin [6] and Borden and Meiburg [8], the flow is energy conserving only for $H^*_{\text{lock}} = 1$, when the left- and right-propagating gravity currents occupy half the depth of the tank. For other values of H^*_{lock}, the flow dissipates energy in the region next to the gravity current, since its height is less than 0.5, as well as in the rarefaction wave, and in the left-propagating bore when $H^*_{\text{lock}} > 0.5$. Note that, on the other hand, the analysis of Shin *et al.* [7] had assumed nondissipative flow along the top wall. The head loss Δ^* has a maximum for $H_{\text{lock}} = H/2$, when the left-propagating

bore begins to form. We reiterate that with the vorticity model, explicit knowledge of H_{lock} is not required in order to write down the governing equations for the gravity current front.

VI. CONCLUSION

The vorticity-based modeling concept for stratified flows was initially introduced by Borden and Meiburg [8,14] for quasisteady conditions. Here we have further extended this approach to flows that are fully unsteady at least in some regions, so they cannot be rendered quasisteady by a change of reference frames. In order to accomplish this, we shifted from the integral control volume balance employed in those earlier investigations to a differential control volume balance for the fully unsteady parts of the flow. Evaluation of the conservation equations for mass and vorticity then required the additional assumption of locally uniform parallel flow within each layer. With this additional assumption, we showed that the unsteady vorticity modeling approach reproduces the two-layer shallow-water equations for the unsteady sections of the flow.

In order to test this unsteady modeling approach, we applied it to the case of partial-depth lock-release flows, for which we can compare with model-based predictions as well as experimental data of other authors and with DNSs conducted as part of the present investigation. Consistent with the shallow-water analysis of Rottman and Simpson [13], the vorticity model demonstrates the formation of a quasisteady gravity current front, a fully unsteady expansion wave, and (for $H^*_{\text{lock}} > 0.5$) a quasisteady propagating bore. When a bore forms, it travels with velocity 0.5 and the interface behind it always is at half the channel depth, independent of the lock height. We demonstrate analytically that such bores are energy conserving. The differential vorticity model furthermore gives predictions for the height and velocity of the gravity current and the bore, as well as for the propagation velocities of the edges of the expansion fan, as functions of the lock height. All of these predictions are seen to be in good agreement with the DNS data and, where available, with experimental results. Since it does not require any energy-based closure assumptions, the vorticity model can be employed for an *a posteriori* analysis of the energetics of the flow. Such an analysis shows lock-release flows to be energy conserving only for the case of a full lock, whereas they are always dissipative for partial-depth locks.

The current extension enables the vorticity-based approach to formulate simplified models for a range of stratified flow fields with at least some fully unsteady regions.

ACKNOWLEDGMENT

We gratefully acknowledge support through NSF Grant No. CBET-1335148. We also acknowledge helpful comments by an anonymous referee.

[1] J. E. Simpson, *Gravity Currents in the Environment and Laboratory* (Cambridge University Press, Cambridge, 1997).
[2] E. J. Hopfinger, Snow avalanche motion and related phenomena, Annu. Rev. Fluid Mech. **15**, 47 (1983).
[3] M. Ungarish, *An Introduction to Gravity Currents and Intrusions* (CRC, Boca Raton, 2010).
[4] E. Meiburg and B. Kneller, Turbidity currents and their deposits, Annu. Rev. Fluid Mech. **42**, 135 (2010).
[5] T. von Kármán, The engineer grapples with non-linear problems, Bull. Am. Math. Soc. **46**, 615 (1940).
[6] T. B. Benjamin, Gravity currents and related phenomena, J. Fluid Mech. **31**, 209 (1968).
[7] J. O. Shin, S. B. Dalziel, and P. F. Linden, Gravity currents produced by lock exchange, J. Fluid Mech. **521**, 1 (2004).
[8] Z. Borden and E. Meiburg, Circulation-based models for Boussinesq gravity currents, Phys. Fluids **25**, 101301 (2013).

[9] C. Pozrikidis, *Introduction to Theoretical and Computational Fluid Dynamics* (Oxford University Press, Oxford, 1996).

[10] C. Härtel, E. Meiburg, and F. Necker, Analysis and direct numerical simulation of the flow at a gravity-current head. Part 1. Flow topology and front speed for slip and no-slip boundaries, J. Fluid Mech. **418**, 189 (2000).

[11] M. M. Nasr-Azadani and E. Meiburg, Gravity currents propagating into shear, J. Fluid Mech. **778**, 552 (2015).

[12] M. A. Khodkar, M. M. Nasr-Azadani, and E. Meiburg, Intrusive gravity currents propagating into two-layer stratified ambients: Vorticity modeling, Phys. Rev. Fluids **1**, 044302 (2016).

[13] J. W. Rottman and J. E. Simpson, Gravity currents produced by instantaneous release of a heavy fluid in a rectangular channel, J. Fluid Mech. **135**, 95 (1983).

[14] Z. Borden and E. Meiburg, Circulation-based models for Boussinesq internal bores, J. Fluid Mech. **726**, R1 (2013).

[15] M. M. Nasr-Azadani and E. Meiburg, TURBINS: An immersed boundary, Navier-Stokes code for simulation of gravity and turbidity currents interacting with complex topographies, Comput. Fluids **45**, 14 (2011).

[16] M. M. Nasr-Azadani, Understanding turbidity currents interacting with complex seafloor topographies: A depth-resolved numerical investigation, Ph.D. thesis, University of California, Santa Barbara, 2013.